Geophys. J. Int. (1997) **130,** 661–668

FIR filter effects and nucleation phases

Frank Scherbaum[1] and Marie-Paule Bouin[2]

[1] *Institut für Allgemeine und Angewandte Geophysik, Ludwig Maximilians Universität München, Theresien-strasse,* 41, 80333 *München, Germany. E-mail: frank@bavaria.geophysik.uni-muenchen.de*

[2] *Department of Earth Sciences, University of Oxford, Parks Road, Oxford,* OX1 3PR, *UK. E-mail: marieb@earth.ox.ac.uk*

Accepted 1997 April 25. Received 1997 April 23; in original form 1997 February 19

SUMMARY

The symmetric impulse response of linear phase Finite Impulse Response (FIR) filters most commonly used in modern seismic recording systems produces precursory signals to impulsive arrivals. These acausal filter-generated artefacts may result in misinterpretations of various onset properties. Prior to any onset interpretation, these effects have to be removed from the seismic record. This can be achieved without loss of bandwidth by post-filtration of the digital seismograms if the filter coefficients and the decimation ratios are known. We have analysed numerous signals from different instruments and sampling rates for precursory phases and found that—in contrast to commonly held beliefs—FIR-filter-related precursory signals are not always easy to recognize visually from their waveform signature. Furthermore, they can exhibit surprisingly similar properties to those reported for nucleation phases, although the majority of nucleation phases reported in the past have been obtained on instruments with a causal response. We demonstrate examples of filter-related precursory signals for events scanning nine orders of moment, from 10^{10} N m to 10^{19} N m. Surprisingly, the lower bound of the artefact durations as a function of seismic moment scales close to the cube root of the seismic moment. We interpret this as being caused by the fact that above a certain seismic moment, the attenuated source signal acts as a causal low-pass filter of a smaller bandwidth than the FIR filter. Assuming an ω^{-2} source model, constant stress drop and an empirical relationship between the maximum artefact duration and the cut-off frequency of the FIR filter, the artefact durations are expected to scale proportional to the 1/2.5 power of the seismic moment, in comparison to 1/3 as proposed for nucleation phases.

Key words: instrumentation, onset properties, waveform analysis.

1 INTRODUCTION

A growing body of evidence suggests that the main *P* phase of microearthquakes (Iio 1992, 1995), as well as of moderate and large earthquakes (Umeda 1990; Ellsworth & Beroza 1995), is often preceded by an interval of low amplitudes. These phases, which have been observed on analogue as well as on digital recordings, have been commonly interpreted as reflecting the early stage of the rupture process. In this sense, they have been baptized nucleation phases. The most striking property of these phases is that their durations scale with the cube root of the seismic moment of the corresponding main event (Ellsworth & Beroza 1995).

While the majority of these results has been obtained based on instruments with a causal response, most modern seismic recording systems contain acausal linear phase FIR filters. Such filters have the desirable property that they do not distort the phase spectrum of the input signal. However, because of their symmetric impulse response, they can generate precursory signals to impulsive seismic arrivals. These filter artefacts can create severe problems for the determination of onset properties such as onset times and onset polarities. In this paper we will demonstrate that FIR filter artefacts can become hard, if not impossible, to identify visually, and that their durations can scale in a smilar manner to the cube-root moment scaling reported for nucleation phases.

2 FIR FILTER EFFECTS IN MODERN DIGITAL SEISMIC RECORDS

In modern high-performance seismic acquisition systems, the continuous input signal is originally sampled at several kilohertz and subsequently decimated to the final sampling rate after digital anti-alias filtering. This permits the use of inexpensive continuous time filters as analogue anti-alias filters.

In addition, part of the quantizaton noise is supressed during this process by the digital anti-alias filter, causing the resolution to increase with increasing decimation ratio. In order not to violate the sampling theorem and to achieve maximum resolution, the digital sampling rate reduction must include a very sharp digital anti-alias filter. Ideally, the digital anti-alias filter has to be a steep, stable filter that causes no distortion of the input signal, at least not within its passband. This requires linear phase filters (Oppenheim & Schafer 1989) that are passing signals without phase distortion except for a constant time shift (linear phase), which can be easily accounted for. If the time shift is zero or is corrected for, the filter is called a zero phase filter. Zero or linear phase filters, however, can only be implemented exactly as FIR filters since they require a physically non-realizable impulse response. Causal filters, on the other hand, will always cause a phase distortion of the input signal, even within the passband of the filter. For that reason, zero phase FIR filters are most commonly used in modern seismic data aquisition systems.

In certain contexts, for example for onset-time determination and also for the investigation of nuncleation phases, it is a severe disadvantage of the symmetric impulse response of zero phase filters that it produces precursory signals to impulsive arrivals. This may cause the misinterpretation of various onset properties. The onset time—if we define it as the time where the signal level exceeds some threshold—of an impulsive signal that has been filtered by a zero phase filter will always be advanced by some amount depending on the width of the main lobe of the filter impulse response. This is illustrated in the top trace of Fig. 1 for a spike at time zero and the decimation filter used in the Refraction Technology seismic recording system 72A-08 while decimating from 100 to 20 Hz. The centre of gravity of the filtered signal appears at time zero, which indicates that the group delay of the filter is zero. If the same spike input signal is filtered by the minimum phase equivalent of the filter used for the top trace, the onset in the noise-free case appears at the proper time while the centre of gravity of the signal is delayed (bottom trace in Fig. 1). In the presence of noise, however, the onset will not be detectable until the signal-to-noise ratio (SNR) is sufficiently large and the onset will be apparently delayed. As a consequence, onset times determined from modern data acquisition systems using zero phase FIR filters are biased towards earlier times, while onset times determined from classical instruments using causal filters are biased towards later times. For impulsive signals, the magnitudes of these time differences may reach non-negligible values for tasks such as earthquake location and seismic tomography, as the example in Fig. 1 demonstrates.

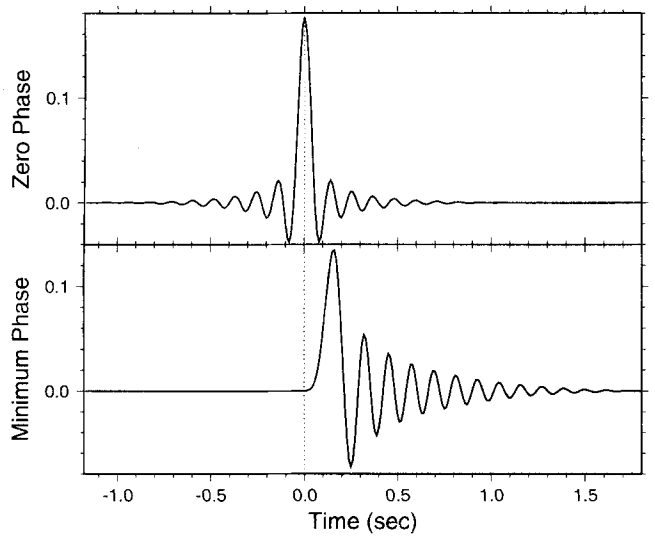

Figure 1. Zero phase and minimum phase equivalent filter. The top trace shows the zero phase FIR filter response (with zeros appended) employed in the last stage of the 72A-08 data aquisition system by Refraction Technology for an input spike at time zero. The bottom trace shows the response of the minimum phase equivalent, that is the filter with the same amplitude frequency response but a minimum phase characteristic.

3 REMOVING THE ACAUSAL RESPONSE OF A ZERO PHASE FIR FILTER

Several methods to suppress or remove FIR-filter-generated precursory artefacts have been reported in the literature (for a discussion see Scherbaum 1996). Since the impulse response of the filter oscillates with the cut-off frequency, a simple pragmatic approach consists of low-pass post-filtration with a causal low-pass filter of smaller bandwidth. This approach, however, is undesirable because it sacrifices signal bandwidth. Furthermore, it only suppresses the oscillatory precursors but leaves ramp-like precursory signals of small amplitudes. In the context of studies of slow initial phases, the resulting signals have a high potential of being misinterpreted.

A method to completely remove the acausal response of a zero phase FIR filter without loss of bandwidth has been proposed by Scherbaum (1996). Following his notation, the FIR-filtered digital seismogram before a particular decimation step can be viewed as

$$\tilde{Y}(z) = F(z)z^{lp}\tilde{X}(z). \tag{1}$$

Here, $\tilde{Y}(z)$ is the z-transform (Oppenheim & Schafer 1989) of $\tilde{y}[n]$, the digitally low-pass filtered seismic trace before decimation and $\tilde{X}(z)$ represents the z-transform of the input signal $\tilde{x}[n]$. $F(z)$ is the z-transform transfer function of a linear phase FIR filter that produces a constant time shift of lp samples. Hence, $F(z)z^{lp}$ is the corresponding zero phase filter in which the linear phase component of $F(z)$ is corrected. For the present purpose we can focus on the treatment of $F(z)$ since the time shift described by z^{lp} can be treated separately.

The transfer function $F(z)$ is the product of a minimum phase component $F_{\min}(z)$ and a maximum phase component $F_{\max}(z)$. The maximum phase component causes the left-sided or 'acausal' part of the impulse response, while the right-sided or 'causal' part corresponds to the minimum phase component. The removal of the acausal response is based on the replacement of $F_{\max}(z)$ by its minimum phase equivalent (MinPhase$\{F_{\max}(z)\}$). This can be carried out by post-filtration of the time-reversed digital seismogram $x'[i]$ using the following difference equation (Scherbaum 1996):

$$y'[i] = \sum_{k=1}^{mx} a[k]y'[i-k] + \sum_{l=0}^{mx} b[l]x'[i-l], \tag{2}$$

with

$$a[k] = \frac{f_{\max}[mx-k]}{f_{\max}[mx]} \qquad \text{for } k = 1 \text{ to } mx \tag{3}$$

and

$$b[l] = \frac{f_{\max}[l]}{f_{\max}[mx]} \qquad \text{for } l = 0 \text{ to } mx. \tag{4}$$

Here, $f_{\max}[l]$ for $l = 0$ to mx are the $mx + 1$ coefficients of the maximum phase portion of the FIR filter. The output sequence $y'[i]$ is the time-reversed sequence for which the non-causal part of the FIR filter has been replaced by its equivalent minimum phase part. After filtering, we can obtain the corrected sequence $y[i]$ by simply flipping $y'[i]$ on the filter output trace. The filter defined by (2) is a pure all-pass filter that preserves the full bandwidth of the seismogram. It produces only a constant onset time advance by lp samples (see eq. 1), which can be corrected for by resetting the time tag of $y[i]$. There are a number of ways to determine the maximum phase portion of the filter. Because of its good performance, here we choose a method based on the determination of the roots of $F(z)$. It is discussed in detail in Scherbaum (1996), together with the full derivation of (2)–(4). The performance of the correction filter can be seen in Fig. 1. The bottom trace in Fig. 1 was actually calculated from the top trace using eq. (2) and correcting for the onset time advance described above.

4 IDENTIFICATION OF FIR-FILTER-GENERATED ARTEFACTS

FIR-filter-related acausal effects are commonly believed to be easily recognizable because of their often monochromatic oscillatory character. An example is shown in Fig. 2(a), where neither the *P* arrival nor the *P* polarity can be read with certainty. However, as can be seen in Fig. 2(b), complex signal character does not automatically rule out FIR filter effects. The comparison between the original seismogram and the corrected trace in Fig. 2(b) clearly shows that the complex precursory signal is purely filter related. Such a signal would be hard, if not impossible, to recognize as filter generated based on its waveform signature alone. In cases where data streams of different sampling rates are available for the same sensor, FIR-filter-related artefacts can be identified to some degree from a comparison of the different data streams. Nevertheless, high-sampling-rate data streams are not spared from FIR filter effects. This is illustrated in Fig. 3, which shows one event recorded on the same station but for two different data streams: 20 Hz and 80 Hz. Note that the filter-generated precursory signal on the uncorrected 20 Hz trace (Fig. 3a) could have been identified as an artefact by comparison with the uncorrected 80 Hz trace (Fig. 3b). However, the nature of the precursory signal on the 80 Hz data stream only becomes clear by comparison with the corrected data. Thus, the only way to safely identify FIR-filter-generated artefacts is by comparison with traces that have not been filtered with acausal filters or from which the acausal effects of the zero phase FIR filter have been removed completely.

5 NUCLEATION PHASES AND FIR FILTER ARTEFACTS

We collected more than 80 examples of precursory phases preceding the main *P* phases of earthquakes of different seismic moments recorded on seven different types of instruments and/or sampling frequencies: Quanterra 80 Hz, Quanterra

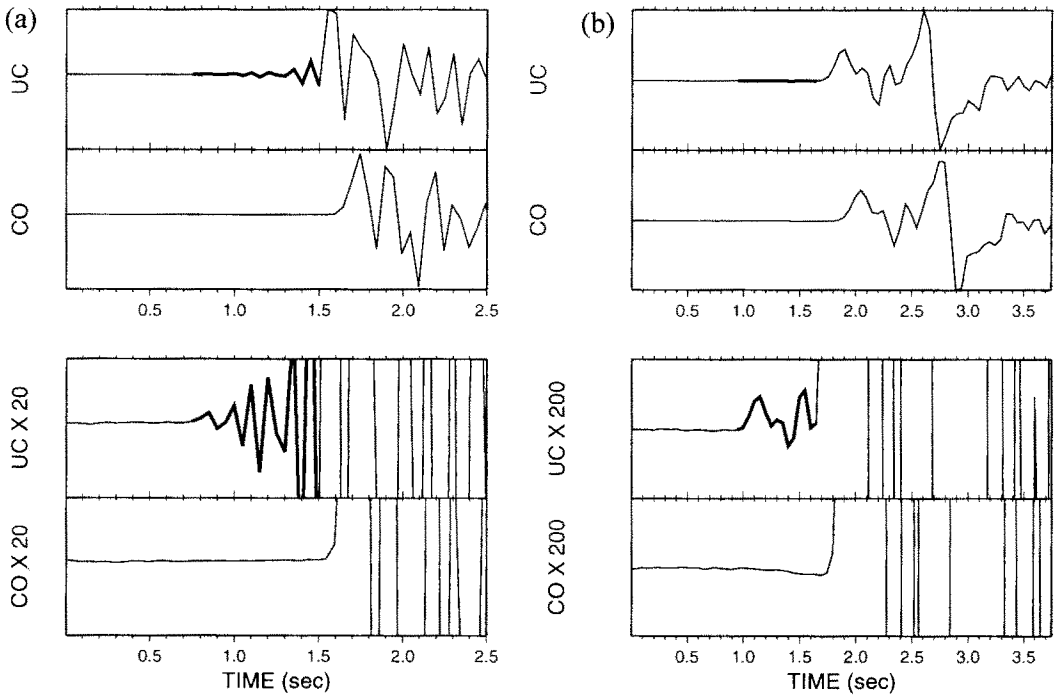

Figure 2. Two examples of FIR filter artefacts of different visual detectibility. Vertical-component *P*-wave records with FIR-filter-generated precursory signals obtained at the stations HUIG (a) and PLIG (b) of the National Mexican Network (STS-2 seismometer, Quanterra data logger, 20 Hz data stream) are shown. From top to bottom the traces are: uncorrected low gain (UC), FIR-filter-corrected low gain (CO), uncorrected high gain (UC × amplification factor) and corrected high gain (CO × amplification factor). The thick-line portions mark FIR filter artefacts. Note the differences in waveform signature of the FIR filter artefacts in (a) and (b).

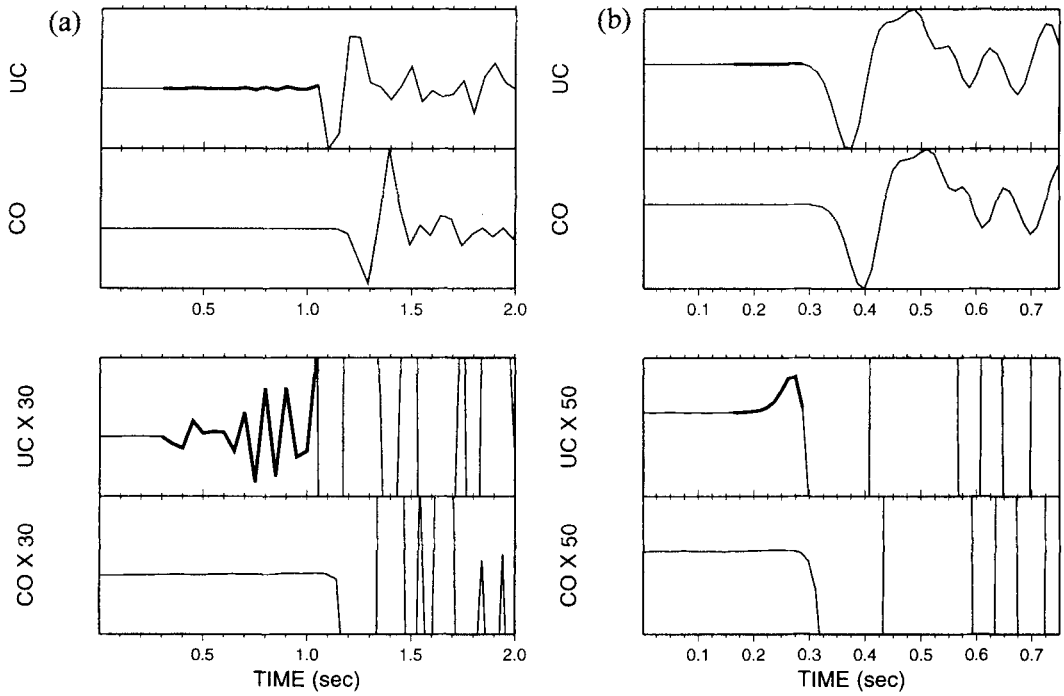

Figure 3. (a) and (b) show the same $M_1 = 4.2$ event recorded at station SGN of the FREESIA (Fundamental Research on Earthquakes and Earth'S Interior Anomalies) network of the NIED (National Research Institute for Earth Science and Disaster Prevention), Japan (STS-1 seimometer, Quanterra data logger). (a) The 20 Hz and (b) the 80 Hz data stream. From top to bottom the traces are: uncorrected low gain (UC), FIR-filter-corrected low gain (CO), uncorrected high gain (UC × amplification factor) and corrected high gain (CO × amplification factor). The thick-line portions mark FIR filter artefacts.

40 Hz, Quanterra 20 Hz, Mars88 125 Hz, Reftek 50 Hz, SIL (Nanometrics) 100 Hz, Titan 1 Hz. They were identified as FIR filter artefacts by a comparison of the original and the corrected traces. In the centre panel of Fig. 4 their durations are plotted as a function of the seismic moment of the corresponding earthquakes. Superimposed are plots of the durations of published nucleation phases, keeping in mind that essentially all of these have been obtained from instruments with a causal response. Most of the artefacts fall above the distribution of the published nucleation phases, with an overall increase of artefact duration with seismic moment. Interestingly, the distribution of the artefacts seems to be bounded by the distribution of the nucleation phases. This can be seen on Fig. 4 for earthquakes scanning approximately nine orders of seismic moment, from 10^{10} N m to 10^{19} N m. No artefacts were found for which the durations fall below the distribution of published nucleation phases. Out of the complete data set, 17 waveform examples are shown to illustrate that—in contrast to commonly held beliefs—the waveforms of FIR filter artefacts can become extremely variable and complex. Fig. 4 shows that in particular those filter-generated precursors whose durations approach the distribution of published nucleation phases become more or less impossible to identify as artefacts simply from visual inspection. As demonstrated, these phases must not be interpreted as nucleation phases, although they share some of their characteristics.

6 SCALING OF ARTEFACT DURATION WITH SEISMIC MOMENT

The overall increase in the duration of FIR filter artefacts with seismic moment is caused primarily by the fact that larger earthquakes are commonly recorded at lower sampling frequencies than smaller ones. This implies longer FIR filter durations and therefore in general longer artefact durations. The banded structure visible for the distribution of artefact duration as a function of seismic moment in Fig. 4 reflects the different instruments/sampling rates. Clearly, the overall pattern is dominated by the two data sets for which we have the most examples, namely the Quanterra 20 Hz and 80 Hz data streams (Fig. 5). For any given data stream there is a different maximum seismic moment for which FIR filter artefacts are observed. We interpret this as being caused by the fact that above a certain seismic moment, the attenuated source signal acts as a causal low-pass filter of smaller bandwidth than the FIR filter. The same effect can be used for the suppression of FIR-filter-generated precursory oscillations by post-filtration with a causal low-pass filter of smaller bandwidth, as was discussed above. In other words, artefacts are only visible if they fall within the passband of the attenuated source signal, that is if ω_{FIR}, the frequency at which the FIR filter oscillates, is smaller than the effective corner frequency, ω_c, of the attenuated source signal. With increasing seismic moment the effective corner frequency ω_c decreases and the amplitudes of the FIR-filter-generated precursory signals become increasingly negligible with respect to the maximum signal amplitude. We simulated this behaviour for the 40 Hz Quanterra data stream using Sato's (1994) source model. We fixed the rupture velocity at 2.6 km s^{-1} ($0.75v_s$ for $v_s = 3.5$ km s^{-1}) and increased the seismic moments from 10^{13} to 10^{22} N m. We considered a single station at a hypocentral distance of 25 km and an angle of 60° between the ray and the fault normal. Attenuation is accomodated by a causal operator assuming a Q value of 100. Resulting synthetic P-wave onsets

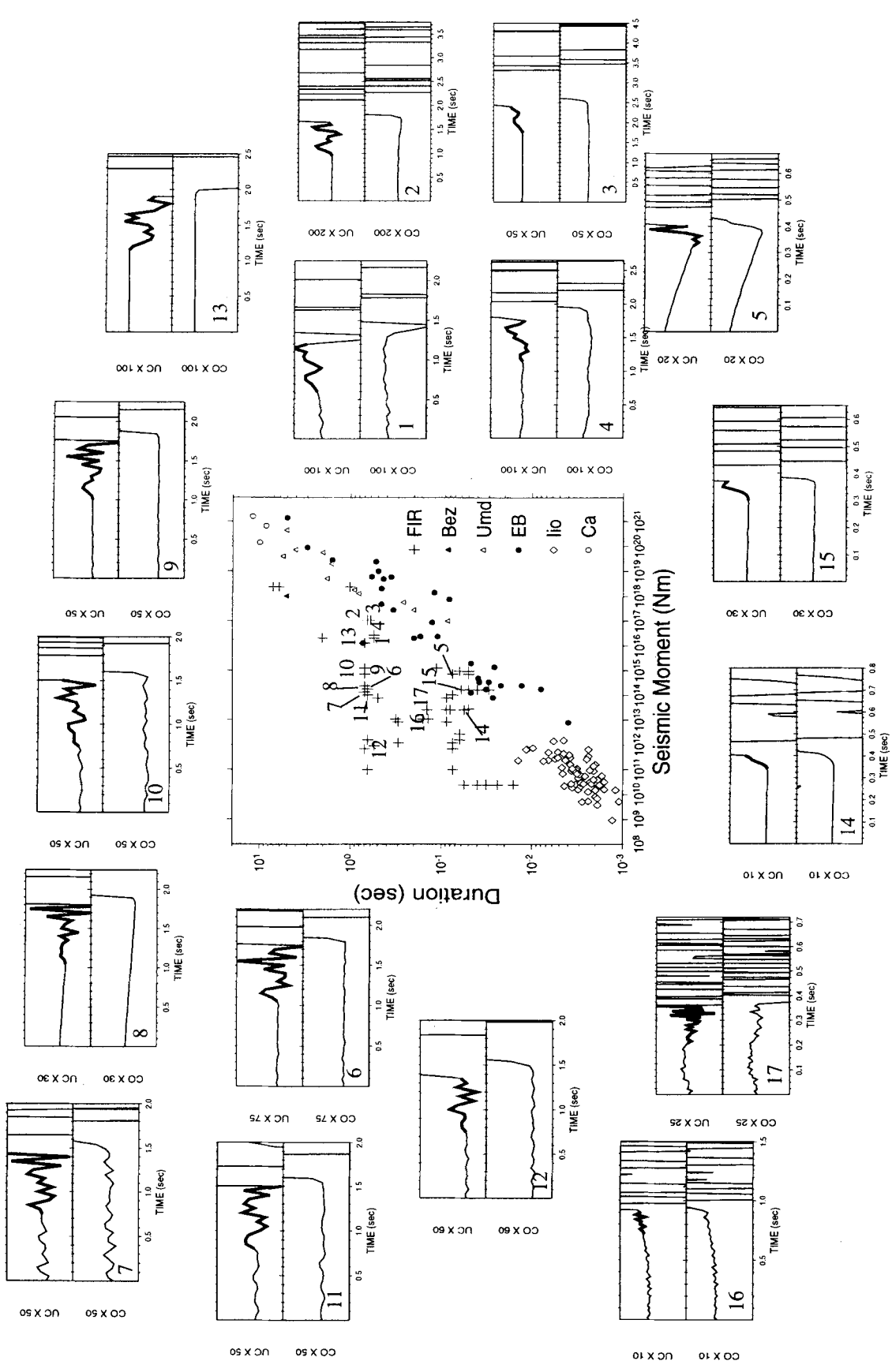

Figure 4. Distribution of durations of FIR filter artefacts (+) as a function of the seismic moment of the corresponding earthquakes. The 17 selected waveform examples were chosen as particularly illustrative examples of signals that from their waveform signature could be easily mistaken as seismic signals. The top trace of each inset shows the original seismogram, while the bottom trace shows the corrected trace. The thick-line portions mark the FIR filter artefacts. In the centre panel, the duration of the precursory FIR filter signals are plotted as + against the seismic moment of the corrsponding events. The numbers at each + correspond to the event numbers of the waveform examples. Superimposed using different symbols are the durations of published nucleation phases. Bez: Bezzeghoud, Deschamps & Madariaga (1986, 1989); Umd: Umeda (1990); EB: Ellsworth & Beroza (1995); Iio: Iio (1995); Ca: Campos *et al.* (1994), Campos & Madariaga (1995) and Campos, Madariaga & Scholz (1996).

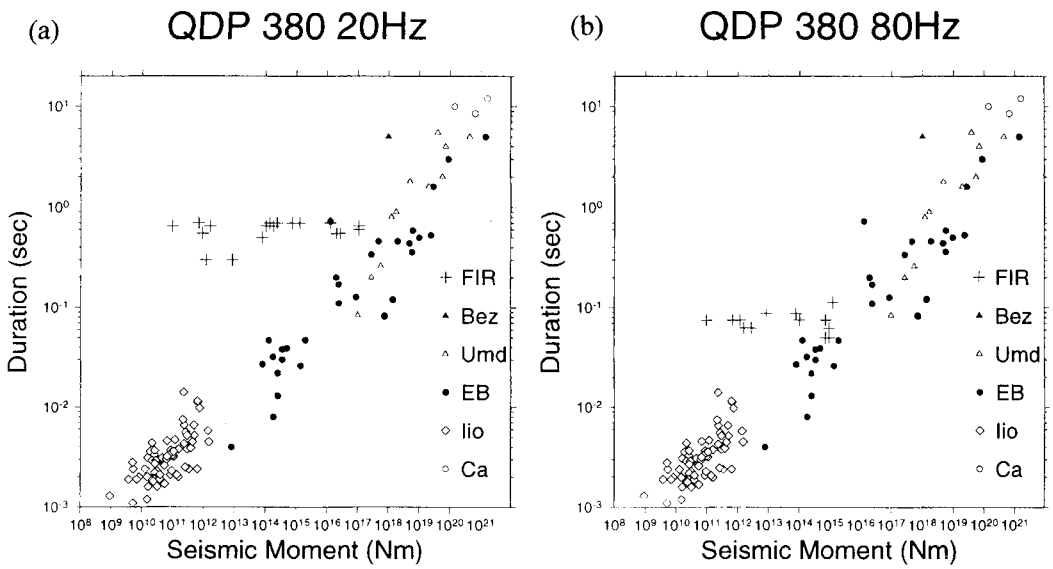

Figure 5. Distribution of precursory FIR-filter-artefact durations for (a) the Quanterra 20 Hz and (b) the Quanterra 80 Hz data streams from Fig. 4.

are plotted in Fig. 6. To facilitate the comparison, we normalized all traces to a maximum amplitude of 1. As a measure of FIR-filter-artefact detectability, the labels on the vertical axis give the maximum amplitude in each panel after normalization. The lowermost trace shows the superposition of the 10 traces above on the same scale. As shown in Fig. 6, the artefacts become less recognizable with increasing seismic moment (from top to bottom), while their amplitudes decrease. Their visible duration will depend on the signal-to-noise ratio, so some scatter is to be expected. For a seismic moment of around 10^{18} N m (trace 6 in Fig. 6), artefact amplitude becomes negligible in our Quanterra 40 Hz data stream simulation.

To approximate the corresponding scaling law quantitatively, let us assume that $M_{0\max}$, the maximum seismic moment for which a FIR-filter-generated precursor is visible, is given by the condition

$$\omega_{\mathrm{FIR}} = \omega_c . \tag{5}$$

Since ω_c is reduced with increasing seismic moment, the amplitudes of the precursory signals become more and more negligible with respect to the maximum signal amplitude (*cf.* Fig. 6). For an ω^{-2} source model and constant static stress drop, the corner frequency ω_c of the source signal scales with the seismic moment M_0:

$$\omega_c \sim M_0^{-1/3} . \tag{6}$$

From condition (5) we see that $M_{0\max}$ will scale with the inverse of the cube of ω_{FIR}:

$$M_{0\max} \sim \omega_{\mathrm{FIR}}^{-3} . \tag{7}$$

Since ω_{FIR} and τ_{FIR} are related, we can directly express $M_{0\max}$ by τ_{FIR}. For this we use the facts that (1) $\omega_{\mathrm{FIR}} \sim F_{\mathrm{dig}}$ (commonly $\omega_{\mathrm{FIR}} = 2\pi 0.4 F_{\mathrm{dig}}$) and (2) based on regression analysis for the instruments considered in Fig. 4, the FIR-filter artefact duration τ_{FIR} scales with data-logger frequencies F_{dig} according to (Fig. 7).

$$\tau_{\mathrm{FIR}} = 31.75 F_{\mathrm{dig}}^{-1.2} . \tag{8}$$

This yields

$$\omega_{\mathrm{FIR}} \sim \tau_{\mathrm{FIR}}^{-0.833} . \tag{9}$$

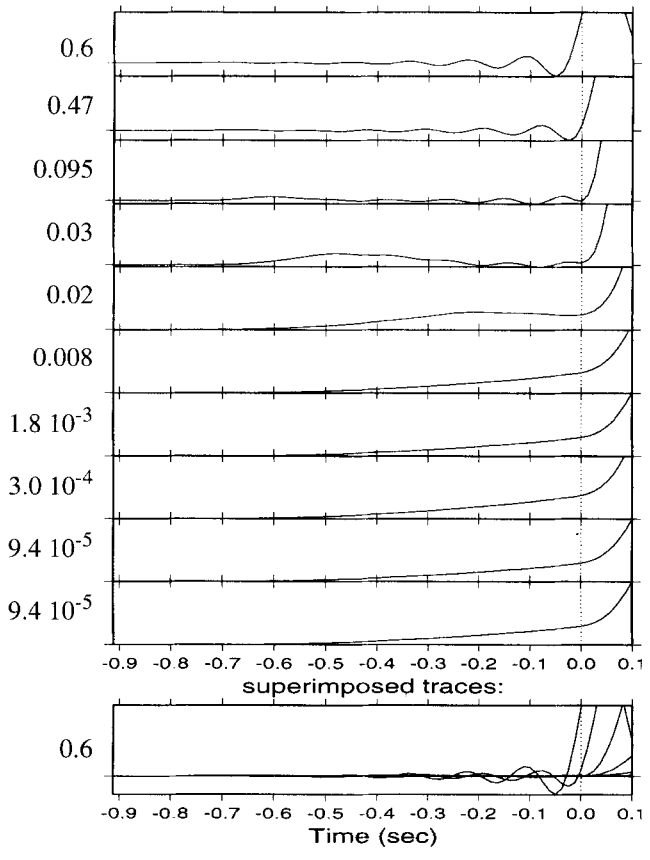

Figure 6. Simulated 40 Hz Quanterra seismograms of synthetic *P*-wave onsets for Sato's (1994) source model for a constant rupture velocity and varying seismic moments. From top to bottom the seismic moments increase from 10^{13} to 10^{22} N m. The maximum trace amplitudes have been normalized to 1. As a measure of FIR-filter-artefact detectability, the labels on the vertical axis give the maximum amplitude in each panel after normalization. The lowermost trace shows the superposition of the 10 traces above on the same scale. The causal onset corresponds to time zero.

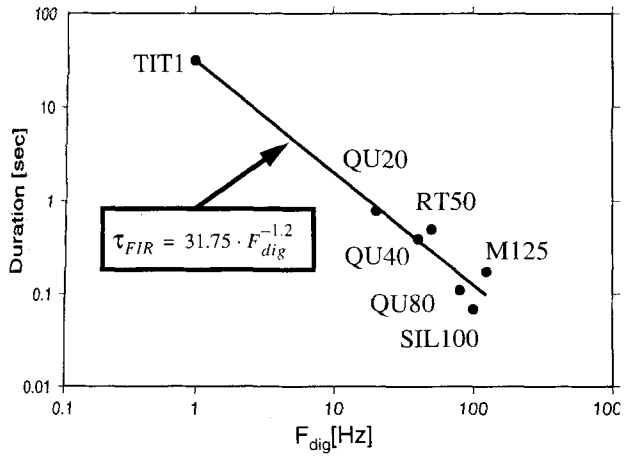

Figure 7. FIR-filter-artefact duration, τ_{FIR}, defined as the length of the left-sided part of the FIR filter impulse response, for the instruments considered in Fig. 4. QU: Quanterra; RT: Reftek; M: Mars88; TIT: Titan; SIL: SIL (Stefánsson *et al.* 1993). The numbers following the data-logger description are the sampling frequencies in Hz.

Inserting eq. (9) into eq. (7) we see that the maximum seismic moment for which a FIR filter artefact will be visible scales with the artefact duration τ_{FIR}:

$$M_{0max} \sim \tau_{FIR}^{2.5}. \tag{10}$$

Therefore, the apparent minimum duration τ_{min} for a given seismic moment scales very similar to the cube-root scaling

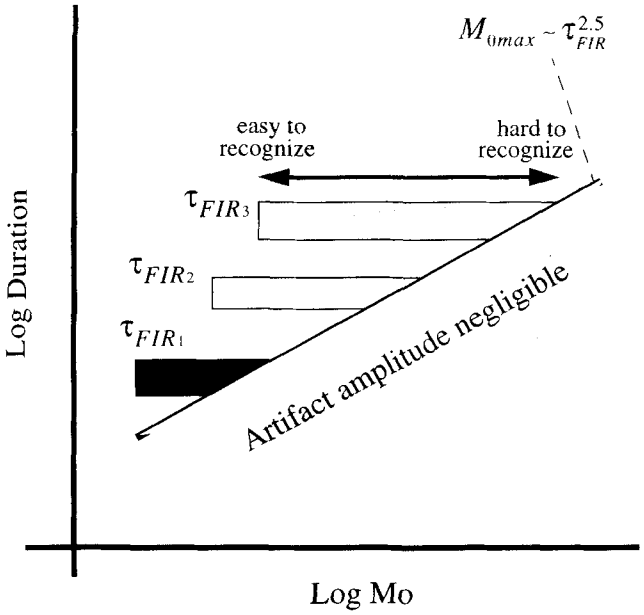

Figure 8. Interpretation of the scaling law of the FIR-filter-artefact durations with seismic moment. The shaded areas labelled τ_{FIR}, τ_{FIR2} and τ_{FIR3} represent the distributions of characteristic artefact durations for three different data streams. With increasing seismic moment, for each data stream the FIR-filter-generated precursory signals become hard to recognize as artefacts until their amplitude becomes negligible. The maximum seismic moment for which the precursory artefacts are of significant amplitude scales with the artefact duration such that $M_{0max} \sim \tau_{FIR}^{2.5}$.

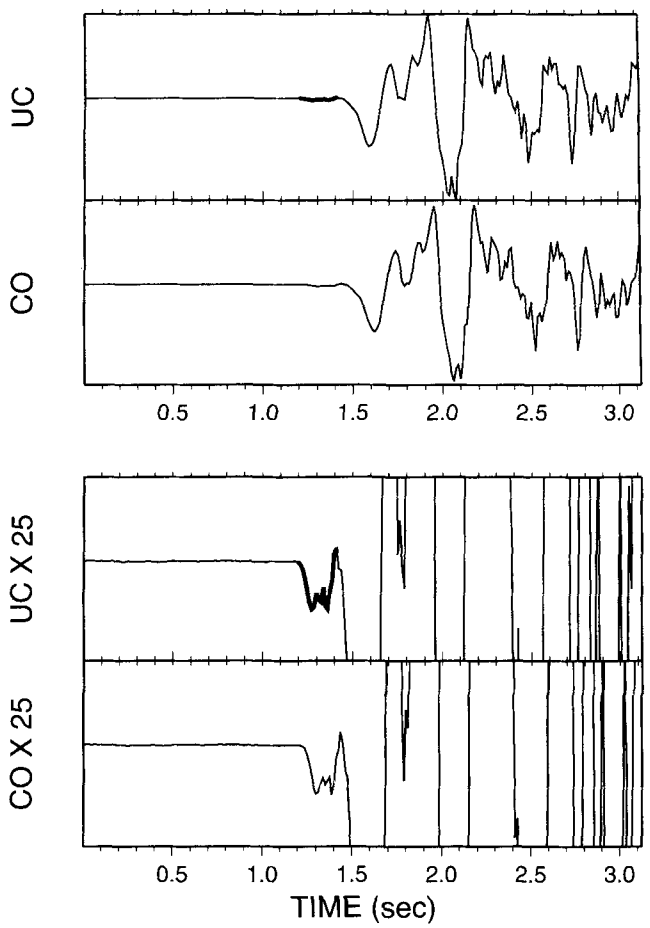

Figure 9. Vertical component of a *P*-wave seismogram recorded at station PNIG of the National Mexican Network that shows clear weak precursory motion even after FIR filter correction. From top to bottom the traces are: uncorrected low gain (UC), FIR-filter-corrected low gain (CO), uncorrected high gain (UC × amplification factor) and corrected high gain (CO × amplification factor). The duration of the precursory signal is 0.22 s (an M_0 value of the main event of 1.5×10^{17} N m was obtained).

observed for the nucleation phases, namely

$$\tau_{min} \sim M_0^{1/2.5}. \tag{11}$$

Therefore, those FIR-filter-related precursory signals that, because of their waveform signature, are most likely to go undetected as instrumental effect are expected to follow nearly a cube-root relationship between their duration and the seismic moment. Fig. 8 summarizes this interpretation.

We want to state clearly that we are not claiming that all reported nucleation phases are artefacts, since most of them have been determined from analogue filtered digitized traces (Ellsworth & Beroza 1995; Umeda 1990). We also want to emphasize that weak precursory seismic motions are maintained through our correction. This is illustrated in Fig. 9. The small complex precursory phase exhibited in the uncorrected trace is still clearly visible after correcting the FIR filter effect. Clearly, this precursor is not FIR filter related.

7 CONCLUSION

We have analysed the properties of FIR-filter-generated precursory phases observed on different seismic recording systems.

Using the method developed by Scherbaum (1996), we have found that FIR-filter-related acausal effects can be removed completely by post-filtration. Weak precursory seismic motion is maintained by this correction.

We have also found that contrary to commonly held beliefs, FIR filter artefacts in many cases become impossible to identify visually. Therefore, any signal onset analysis from data loggers using linear phase FIR filters must be preceded by a correction of the acausal filter effects.

If data from different instruments and/or sampling rates are combined, the situation becomes especially dangerous for nucleation phase studies. In particular, those FIR filter artefacts that are hard to recognize can exhibit surprisingly similar scaling properties to the cube-root moment scaling suggested for nucleation phases.

In conclusion, we want to emphasize that nucleation phases can only be detected on modern digital recordings systems if extreme care is taken to remove any FIR-filter-related acausal effects properly. These artefacts can create severe problems for the determination of onset times and polarities. Although in this study we have focused on potential problems for nucleation phase studies, some of the effects illustrated apply in a much wider context, for example to earthquake location and seismic tomography.

ACKNOWLEDGMENTS

We have benefited from discussions with Bill Ellsworth, Greg Beroza, Nicolas Deichmann, Andreas Rietbrock and Steinunn Jakobsdottir. We are indebted to Nicolas Deichmann for his code to synthesize Sato's (1994) source model (Deichmann 1997) and to Erhard Wielandt for his interpolation routines. Greg Beroza and Bill Ellsworth provided us with identified and avoided FIR filter artefacts. We would like to acknowledge the numerous people who have provided data for this study (in alphabetical order): Greg Beroza, Wolfgang Bruestle, Hans-Albert Dahlheim, Anne Deschamps, Nicolas Deichmann, Bill Ellsworth, Jim Fowler, Eiichi Fukuyama, Steinunn Jakobsdottir and Mladen Zivcic.

REFERENCES

Bezzeghoud, M., Deschamps, A. & Madariaga, R., 1986. Broad-band modeling of the Corinth, Greece earthquakes of February and March 1981, *Ann. Geophys.*, **4-B,** 295–304.

Bezzeghoud, M., Deschamps, A. & Madariaga, R., 1989. Broad-band P-wave signals and spectra from digital stations, in *Digital Seismology and Fine Modeling of the Lithosphere,* pp. 351–374, eds Casinis, R., Nolet, G. & Panza, G.F., Plenum Press, New York, NY.

Campos, J. & Madariaga, R., 1995. Abrupt initialisation of rupture for the $M_w = 8.1$ earthquake of July 30, 1995 in Antofagasta, Chile, *EOS, Trans. Am. geophys. Un.,* **46,** 76.

Campos, J., Madariaga, R., Nabelek, J., Bukchin, B.G. & Deschamps, A., 1994. Faulting process of the 20 June 1990 Iran earthquake from broadband records, *Geophys. J. Int.,* **118,** 31–46.

Campos, J., Madariaga, R. & Scholz, C., 1996. Faulting process of the August 8, 1993 Guam Earthquake: a thrust event in an otherwise weakly coupled subduction zone, *J. geophys. Res.,* **101,** 17 581–17 596.

Deichmann, N., 1997. Far field pulse shapes from circular sources with variable rupture velocity, *Bull. seism. Soc. Am.,* in press.

Ellsworth, W.L. & Beroza, G.C., 1995. Seismic evidence for an earthquake nucleation phase, *Science,* **268,** 851–855.

Iio, Y., 1992. Slow initial phase of the P-wave velocity pulse generated by microearthquakes, *Geophys. Res. Lett.,* **19,** 477–480.

Iio, Y., 1995. Observations of the slow initial phase generated by micro-earthquakes: Implications for earthquake nucleation and propagation, *J. geophys. Res.,* **100,** 15 333–15 349.

Oppenheim, A.V. & Schafer, R.W., 1989. Discrete-time signal processing, *Prentice Hall,* Englewood Cliffs, NY.

Sato, T., 1994. Seismic radiation from circular cracks growing at variable rupture velocity, *Bull. seism. Soc. Am.,* **84,** 1199–1215.

Scherbaum, F., 1996. *Of Poles and Zeros: Fundamentals of Digital Seismology,* Kluwer, Dordrecht.

Stefánsson, R. *et al.* 1993. Earthquake prediction research in the South Iceland Seismic Zone and the SIL project, *Bull. seism. Soc. Am.,* **83,** 696–716.

Umeda, Y., 1990. High amplitude seismic waves radiated from the bright spot of an earthquake, *Tectonophysics,* **175,** 81–92.